High-order above-threshold dissociation of molecules

Peifen Lu[a,1], Junping Wang[b], Hui Li[a], Kang Lin[a], Xiaochun Gong[a], Qiying Song[a], Qinying Ji[a], Wenbin Zhang[a], Junyang Ma[a], Hanxiao Li[a], Heping Zeng[a], Feng He[b,c,1], and Jian Wu[a,d,1]

[a]State Key Laboratory of Precision Spectroscopy, East China Normal University, 200062 Shanghai, China; [b]Key Laboratory of Laser Plasmas (Ministry of Education), School of Physics and Astronomy, Shanghai Jiao Tong University, 200240 Shanghai, China; [c]Collaborative Innovation Center for Inertial Fusion Sciences and Applications (CICIFSA), Shanghai Jiao Tong University, 200240 Shanghai, China; and [d]Collaborative Innovation Center of Extreme Optics, Shanxi University, Taiyuan, 030006 Shanxi, China

Edited by Margaret M. Murnane, University of Colorado at Boulder, Boulder, CO, and approved January 17, 2018 (received for review November 9, 2017)

Electrons bound to atoms or molecules can simultaneously absorb multiple photons via the above-threshold ionization featured with discrete peaks in the photoelectron spectrum on account of the quantized nature of the light energy. Analogously, the above-threshold dissociation of molecules has been proposed to address the multiple-photon energy deposition in the nuclei of molecules. In this case, nuclear energy spectra consisting of photon-energy spaced peaks exceeding the binding energy of the molecular bond are predicted. Although the observation of such phenomena is difficult, this scenario is nevertheless logical and is based on the fundamental laws. Here, we report conclusive experimental observation of high-order above-threshold dissociation of H_2 in strong laser fields where the tunneling-ionized electron transfers the absorbed multiphoton energy, which is above the ionization threshold to the nuclei via the field-driven inelastic rescattering. Our results provide an unambiguous evidence that the electron and nuclei of a molecule as a whole absorb multiple photons, and thus above-threshold ionization and above-threshold dissociation must appear simultaneously, which is the cornerstone of the nowadays strong-field molecular physics.

above-threshold dissociation | electron–nuclear correlation | inelastic rescattering | coincidence measurement

In 1905, Albert Einstein proposed the hypothesis of light quanta, which postulates that light energy is carried in discrete quantized packets (photons), to explain the law of photoelectric effect. This has been a pivotal step in understanding of the quantized nature of light. Since then, studies of photoionization in strong fields have been greatly boosted and various mechanisms have been understood, e.g., the multiphoton and tunneling ionizations. In 1979, above-threshold ionization (ATI) was observed in the multiphoton ionization of atoms exposed to strong laser fields (1). Multiple photons with energy exceeding the ionization threshold can be simultaneously absorbed, leading to discrete photoelectron spectra on account of the quantized nature of the multiphoton energy absorption. Similarly to ATI, above-threshold dissociation (ATD) (2) was predicted for the multiphoton dissociation of molecules in strong laser fields. In the process of ATD, typically the number of absorbed photons exceeds the minimum required for breaking the molecular bond, appearing as evenly spaced peaks in the kinetic energy release (KER) spectrum of the nuclear fragments.

Despite the fact that the existence of ATD is logical and consistent with fundamental laws of nature, the experimental evidence of the distinct high-order (more than three orders) ATD has never been reported while the theoretical prediction was made more than 20 years ago (2). An early experiment using 532-nm, 100-ps laser pulses showed the first signature of the third-order ATD of H_2^+ due to the photon-coupled dipole transition between the $1s\sigma_g$ and $2p\sigma_u$ states (3). Since then, significant efforts have been dedicated to enhance the experimental visibility of the high-order ATD of molecules by, e.g., using vibrational cold molecular ions (4) or applying intense few-cycle laser pulses (5). Nevertheless, the observation of the distinct ATD spectra is still an open question.

The essential problem of concealing the distinct high-order ATD lies on the electron–nuclear correlation in molecular dissociative ionization. The photon energy absorbed by a molecule is shared between the electronic and nuclear degrees of freedom, which implies that the ATD could not be revealed if the freed electron is not measured in coincidence with the nuclear fragments (4–7). Previous coincidence measurements of dissociative ionization of molecules in femtosecond UV laser pulses explicitly showed the correlation between electron and nuclear degrees of freedom but no high-order ATD spectrum was observed (8–10). Here we pursue an alternative route to observe high-order ATD by taking advantage of the joint energy spectrum (JES) (8–14) of the coincidently measured electron and ion ejected from the same molecule. In particular, the correlated dynamics of the liberated electron and nuclei are bridged by laser-driven inelastic rescattering and can be unveiled by the electron–nuclear JES, which indicates that the electron and nuclei of the molecule as a whole absorb the multiphoton energy. Similarly to the ATI photoelectron spectrum, more than four distinct peaks spaced by the photon energy are observed in the nuclear KER spectrum, which is an unambiguous evidence of high-order ATD. Numerical simulations allow us to trace the periodical emission of the correlated electron–nuclear wave packets in each optical cycle, leading to the coexistence of the discrete ATI and ATD spectra in the dissociative ionization of molecules.

Significance

Above-threshold ionization of atoms in strong laser fields is extensively studied for its overwhelming importance and universality. However, its counterpart, above-threshold dissociation of molecules in strong laser fields, is hard to be observed, although it has been predicted for decades. In this paper, by measuring the momenta of photoelectron and dissociative fragments coincidently, we successfully obtained distinct nuclear energy peaks of the high-order above-threshold dissociation, which must appear simultaneously with the above-threshold ionization. The coexistence of high-order above-threshold dissociation and high-order above-threshold ionization in molecular dissociative ionization offers a perspective to disentangle the complex electron–nuclear correlation in molecules and to image the molecular orbitals, and so on.

Author contributions: P.L., Hui Li, K.L., X.G., Q.S., Q.J., W.Z., J.M., Hanxiao Li, H.Z., and J. Wu contributed to the experiment and analysis; J. Wang and F.H. contributed the theoretical simulation; and P.L., J. Wang, F.H., and J. Wu wrote the paper.

The authors declare no conflict of interest.

This article is a PNAS Direct Submission.

[1]To whom correspondence may be addressed. Email: pflu@lps.ecnu.edu.cn, fhe@sjtu.edu.cn, or jwu@phy.ecnu.edu.cn.

This article contains supporting information online at www.pnas.org/lookup/suppl/doi:10.1073/pnas.1719481115/-/DCSupplemental.

Published online February 13, 2018.

Results and Discussion

Hydrogen and its isotopes, as the simplest neutral molecule, have been the prototype for understanding fundamental molecular processes (3, 15, 16). Here, H_2 molecule is used to demonstrate the ATD of molecules in strong laser fields, that is, $H_2 + n\hbar\omega \rightarrow H^+ + H + e$, hereafter denoted as $H_2(1,0)$ channel. In this paper, we focus on the electron rescattering-assisted ATD, as illustrated in Fig. 1*A*. One electron is freed via the tunneling through the laser-dressed Coulomb potential, while, the generated molecular ion H_2^+ starts to stretch along the potential surface of the $1s\sigma_g$ state. The accelerated electron in the laser field may slam back and transfer its energy to H_2^+, launching the nuclear wave packet onto the $2p\sigma_u$ state, which dissociates afterward into the nuclear fragments with high kinetic energies. Such rescattering events occur periodically in every optical cycle. In the experiment, linearly polarized laser pulses (100 fs, 790 nm) with a peak intensity of 9×10^{13} W/cm^2 were utilized. The measurements were performed in a reaction microscope setup of the cold target recoil ion momentum spectroscopy (17, 18) (*Materials and Methods*). The proton H^+ and the correlated electron e from $H_2(1,0)$ channel were detected in coincidence measurement. The total KER of the nuclei (E_N), that is, the sum of the kinetic energy of the proton (E_p) and the hydrogen atom (E_H), was deduced based on the momentum conservation of the breaking system.

Fig. 2*A* depicts the measured electron–nuclear JES, that is, the yield of $H_2(1,0)$ channel as a function of the photoelectron energy (E_e) and the nuclear kinetic energy (E_N), using linearly polarized laser fields. Two distinct regions separated at about $E_N \sim 2$ eV can be recognized, which can be attributed to different dissociation mechanisms. The low-E_N region (with $E_N < 2$ eV) originates from one-photon and net two-photon transitions between the $1s\sigma_g$ and $2p\sigma_u$ states of H_2^+, which has been widely studied both theoretically and experimentally (19–24). However, the high-E_N region (with $E_N > 2$ eV) is mainly produced via electron recollision, which we will focus on in the following discussion. The rescattering nature of the high-E_N pathway is verified by adjusting the polarization of the driving laser from linear to circular. As shown in Fig. 2*B*, the high-E_N pathway is dramatically suppressed in the circularly polarized light (blue curve) compared with the linearly polarized case (red curve) (see *SI Text* for the electron–nuclear JES in circularly polarized laser fields). The circularly polarized light produces very few events with E_N in the range of 2–6 eV which originate mainly from the Coulomb explosion via the charge-resonance enhanced double ionization of H_2 rather than the dissociative single-ionization channel of $H_2(1,0)$ which we focus on here for the observation of the high-order ATD.

To reveal the underlying mechanism of the rescattering-bridged JES, we numerically simulate the time-dependent Schrödinger equations by including two-electron dynamics and nuclear vibration along the laser polarization axis (*Materials and Methods*). The calculated JES is shown in Fig. 2*D*, which shares very similar structures with the experimental results shown in Fig. 2*A*, especially in the high-E_N region. To confirm that the dissociation of H_2^+ in the high-E_N region is triggered by the electron rescattering rather than the photon resonant coupling between the $1s\sigma_g$ and $2p\sigma_u$ states, we omitted the laser-e_2 coupling and diagnosed the wave packet corresponding to $H_2(1,0)$. This gives almost unchanged high-E_N JES but yields a substantially suppressed low-E_N JES (see *SI Text* for details). It clearly indicates the capability of our one-dimensional model to simulate the role of rescattering in producing the high-E_N JES,

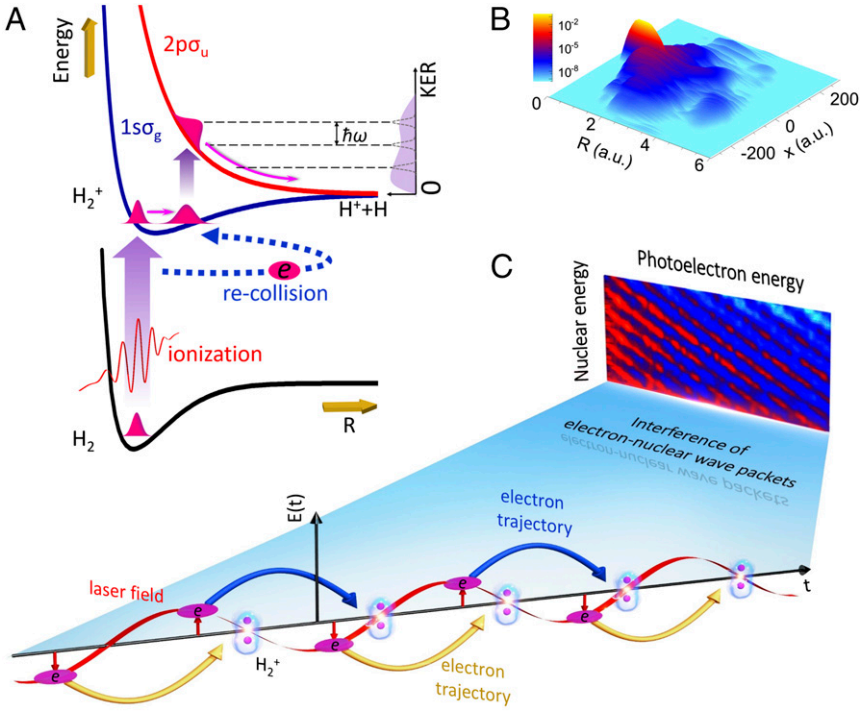

Fig. 1. (*A*) Potential energy curves related to the dissociative ionization of H_2 molecules. The electron tunneling out the laser-dressed Coulomb potential around the peak of the laser electric field is accelerated in the remaining laser field. When the energetic electron recollides with its parent ion, it transfers the absorbed photon energy to the ion by exciting H_2^+ from $1s\sigma_g$ to $2p\sigma_u$ state, resulting in the dissociation afterward of H_2^+. (*B*) The snapshot of wave-packet distribution in R–x space, where R is the internuclear distance of H_2^+ and x specifies the position of the ejected electron wave packet propagating along the polarization direction of the laser field. (*C*) The periodical rescattering-induced correlated electron–nuclear wave packets in every optical cycle interfere with each other, contributing to the coexistence of the ATI and ATD. The strong correlation among the freed electron and the dissociative nuclei suggests that the coincident measurement of the electron and nuclear fragments must be assured to observe the distinct high-order ATD.

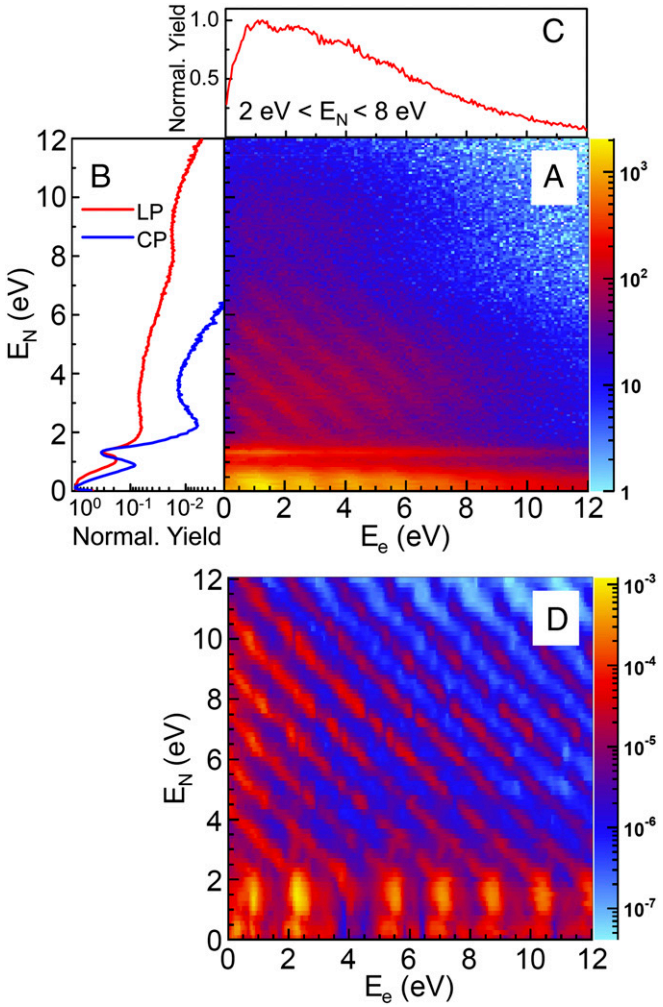

Fig. 2. (*A*) Measured electron–nuclear JES of the $H_2(1,0)$ channel in linearly polarized 790-nm laser pulses with a peak intensity of $I_0 = 9.0 \times 10^{13}$ W/cm^2. (*B*) Nuclear kinetic energy spectra for dissociation of H_2 by linearly polarized (LP, red curve) and circularly polarized (CP, blue curve, $I_0 = 1.8 \times 10^{14}$ W/cm^2) light. (*C*) Photoelectron spectrum of the $H_2(1,0)$ channel with E_N in the range of 2–8 eV in linearly polarized light. (*D*) Calculated electron–nuclear JES of $H_2(1,0)$ in linearly polarized 790-nm laser pulses with a peak intensity of $I_0 = 9.0 \times 10^{13}$ W/cm^2.

although it cannot deal with the dissociative ionization of H_2 in the circularly polarized laser pulses.

As presented in Fig. 2 *B* and *C*, both the nuclear and photoelectron spectra of the high-E_N region exhibit smooth distributions regardless of the quantized nature of the light energy. However, the JES in Fig. 2*A* is featured with multiple diagonal energy correlation lines spaced by the photon energy. This indicates that the electron and nuclei absorb photons as a whole, and the ATI and ATD must be measured simultaneously in the dissociative ionization of molecules. Thus, as shown in Fig. 3*A*, discrete peaks can be reconstructed in the total energy spectrum of all emitted photoelectron and nuclear fragments, that is, $E_{sum} = E_N + E_e$. Furthermore, the ATI (ATD) peaks in the photoelectron (nuclear) spectra can be produced by confining the nuclear (photoelectron) energy in a relatively narrow range. For instance, as shown in Fig. 3*B*, by integrating the electron–nuclear JES over E_N in the range of 3.8–4.2 eV, discrete ATI peaks appear in the photoelectron spectrum. On the other hand, by integrating the electron–nuclear JES over E_e in the range of 0.8–1.2 eV, a photon-energy spaced discrete structure appears in the nuclear spectrum, as shown in Fig. 3*C*. Thus, multiple photon energy exceeding the dissociation threshold is deposited into the nuclei. As shown in Fig. 3 *B* and *C*, the discrete energy of the photoelectron (nuclei) decreases when the nuclear (photoelectron) energy increases owing to their energy sharing of the absorbed photons.

We note that the above-mentioned high-order ATD accessed via the electron recollision differs from the three-photon or the net two-photon ATD explored previously (3, 5) in a fundamental manner. In the previously reported works, most energy of the absorbed photons above the ionization threshold is taken by the electron in the ionization step; while the energy gain of the nuclei originates mainly from the succeeding dipole-allowed photon transitions between $1s\sigma_g$ and $2p\sigma_u$ states. The ionization step and the dissociation step are thus separated. Our present results also differ from the ATD using the cold ion source HD^+ (4), where the HD^+ directly absorbs several photons and then dissociates. In our case, the rescattering of the electron wave packet with the parent H_2^+ launches the dissociative wave packet on the $2p\sigma_u$ state, and the rescattering occurs at every half of the optical

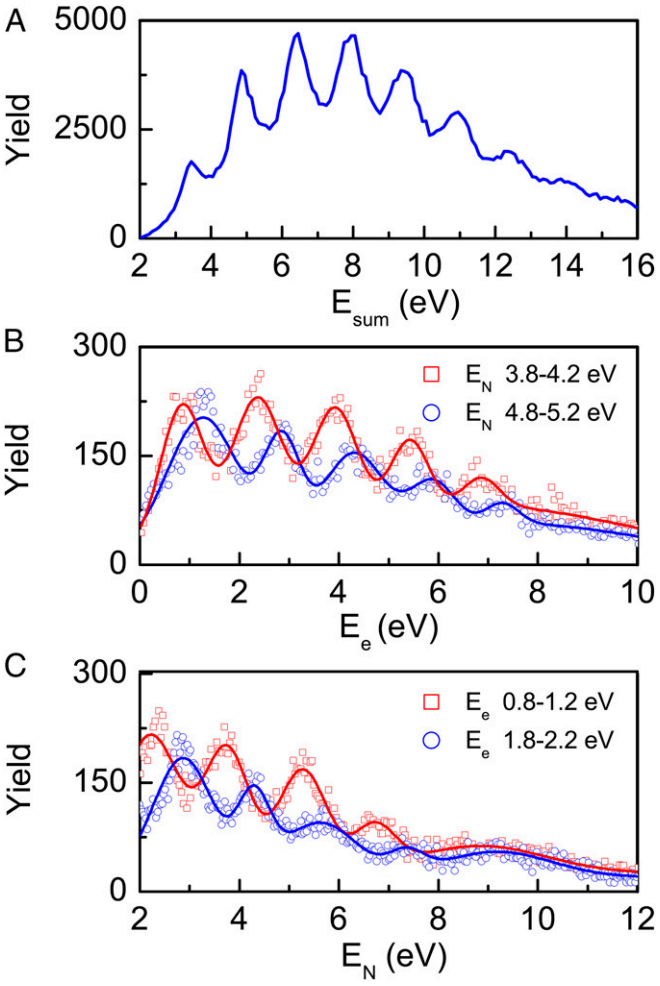

Fig. 3. (*A*) Sum kinetic energy of the coincidently measured nuclei and photoelectron of the $H_2(1,0)$ channel with E_N in the range of 2–8 eV in linearly polarized light. (*B*) Photoelectron spectra obtained by integrating the electron–nuclear JES over E_N in the ranges of 3.8–4.2 eV and 4.8–5.2 eV; and (*C*) nuclear spectra obtained by integrating the electron–nuclear JES over E_e in the ranges of 0.8–1.2 eV and 1.8–2.2 eV for the rescattering-induced dissociation of H_2. The solid curves are numerical fits of the measured data.

cycle. Thus, the dissociative ionized wave packet can be approximately written as

$$\Psi(R,x_1,x_2;t)=\sum\nolimits_j \chi_j(R,x_1;t)\otimes\phi_j(x_2;t),$$

where j indexes the jth rescattering, R, x_1, x_2 specify the internuclear distance and the coordinates of the two electrons along the light polarization direction, $\chi_j(R,x_1;t)$ is the wave packet of the dissociative H_2^+, and $\phi_j(x_2;t)$ describes the wave packet of the rescattered electron. $\Psi(R,x_1,x_2;t)$ should satisfy the two-electron exchanging symmetry since the two electrons form the singlet spin state. Note that the neighboring nuclear wave packets $\chi_j(R,x_1;t)$ and $\chi_{j+1}(R,x_1;t)$ do not interfere with each other since the corresponding electronic parts $\phi_j(x_2;t)$ and $\phi_{j+1}(x_2;t)$ finally propagate in the opposite direction. The interference of every other rescattering molecular wave packet, that is, the intercycle interference (25, 26), induces the joint ATI and ATD. By comparing the high-order ATD with the well-understood nonsequential double ionization of atoms in strong laser fields (27–29), one may find the correspondence between these two scenarios: The tunneling electron rescatters with its parent ion, and shares its energy with another electron. In molecules, the extra freedom of nuclear repulsion finally inherits the energy stored in H_2^+ by inelastic rescattering

There is also a certain probability that the inelastic-rescattering excited H_2^+ is further ionized by the remaining laser field through the charge-resonance enhanced ionization (30, 31) at a critical range of the internuclear distance. Governed by the energy conservation, the slopes of the energy correlation lines in the JES of one electron and two nuclei are expected to be −1 for single ionization and −2 for double ionization if the two electrons have the same energy. The slopes of energy correlation lines in Fig. 2*A* clearly indicate that the high E_N in our measured JES is dominated by the rescattering-induced dissociative single ionization rather than the double-ionization channel, although the two channels may have the overlapping KER distributions.

For the rescattering driven by the oscillating laser field, the electron liberated in the single ionization may revisit the parent ion H_2^+ several times before it is eventually released. During this time interval, the ionization-created vibrational wave packet propagates dispersively on the $1s\sigma_g$ potential energy surface. Different rescattering returns give rise to different KERs of the emitted nuclear fragments. For a given number of absorbed photons, the energy deposition between the electron and correlated nuclei is determined by the internuclear separation at the time of electron recollision. The nuclear wave packet with smaller internuclear separation tends to obtain more energy from the recolliding electron, giving rise to dissociative fragments with higher kinetic energy. The vibrational wave packet is broadened at the time of the third-return recollision, thus resulting in a broader nuclear KER distribution. This accounts for the two bands with E_N in the ranges of 2–8 eV and 8–12 eV in the JES (Fig. 2*A*), which correspond to the two rescattering returns around the internuclear separations of 2.0–3.6 a.u. and 1.7–2.0 a.u., respectively. Our numerical simulations show that the fragments with low KER have larger proportion for a lower laser intensity since the first rescattering does not bring enough energy to excite H_2^+ from $1s\sigma_g$ to $2p\sigma_u$ at small internuclear distances. The multiple rescattering in the dissociation of molecules has also been discussed in the former works (32–34). For the electron rescattering-induced dissociation in the current experiment, the kinetic energy band of 2–8 eV is dominated by the third-return recollision and the kinetic energy band of 8–12 eV is attributed to the first-return recollision.

Conclusion

In conclusion, we have presented a conclusive experimental evidence of the high-order ATD featured with the discrete nuclear energy spectrum by means of JES of the coincidently measured electron and nuclei ejected from the same molecule. High-order ATD of H_2^+ occurs via the energy sharing during the electron-ion inelastic rescattering, instead of the direct absorbing photons from the external laser field. Similarly to the well-observed ATI photoelectron spectrum in multiphoton ionization of atoms, periodical emission of the correlated electron and nuclear wave packets in each optical cycle imprints the quantized nature of the light in the joint ATI and ATD spectra of molecules. The phenomenon of electron rescattering-assisted high-order ATD is expected to be general for various molecules (see *SI Text* for the results of D_2 molecules for instance). However, in the multielectron system, the high energy nuclei depends on the final repulsive electronic state involved in the rescattering-induced excitation of the molecular cation, which might also be influenced by the complex nuclear dynamics when polyatomic molecules are involved. Our results show that the multiparticle correlation in molecules plays key roles in molecular fundamental processes, and the coincidence observation of different fragments in chemical reactions is favor to unveil unambiguously the underlying fascinating dynamics.

Materials and Methods

Experimental Technique. The measurements were performed in an ultrahigh-vacuum reaction microscope setup of the cold target recoil ion momentum spectroscopy (COLTRIMS) (17, 18), where the electrons and ions ejected from a single molecule can be detected in a coincidence measurement by two time- and position-sensitive detectors at the opposite ends of the spectrometer. A beam of linearly polarized femtosecond laser pulses (100 fs, 790 nm, 10 kHz) was down-collimated (2:1) and focused afterward onto a supersonic gas jet of H_2 by a concave silver mirror (f = 75 mm) inside the COLTRIMS. The polarization of the laser pulses can be adjusted to be circular by using a quarter-wave plate. The peak intensity in the laser–molecule interaction zone was estimated to be 9.0×10^{13} W/cm^2 by tracing the intensity-dependent hydrogen's time-of-flight spectrum (35). The maximum kinetic energy of the returning electron is $3.17U_p \sim 16$ eV, which is sufficient to excite the ground state $1s\sigma_g$ to the first excited state $2p\sigma_u$ of H_2^+ but less than the double-ionization threshold. Here, U_p is the ponderomotive energy of the electron in the oscillating laser field. The count rate was ∼0.03 ions and 0.06 electrons per laser shot, which ensures a negligible fraction of the false coincidence among the detected electrons and ions. Three-dimensional momenta of the ejected electrons and protons were reconstructed using the measured times-of-flight and positions of the impacts during the offline analysis. The momentum of the undetected neutral H was deduced based on the momentum conservation of the breaking system, whose kinetic energy together with that of H^+ accounted for the total energy of the nuclei, that is, $E_N = E_p + E_H$.

Theoretical Methods. We solved numerically the time-dependent Schrödinger equation for dissociative ionization of H_2 [atomic units (a.u.) are used] (36, 37)

$$i\frac{\partial}{\partial t}\Psi(R,x_1,x_2;t)=\left[\frac{P_R^2}{2\mu}+\frac{[p_1+A(t)]^2}{2}+\frac{[p_2+A(t)]^2}{2}+V(R,x_1,x_2)\right]\Psi(R,x_1,x_2;t),$$

where μ is the reduced nuclear mass, p_R, p_1, and p_2 are the nuclear relative momentum operator, the first and second electron momentum operators, respectively. $A(t)=-\int_0^t E(t')dt'$ is the laser vector potential with $E(t)$ being the laser electric field. The potential $V(R,x_1,x_2)$ is modified by two R-dependent soft-core parameters (36), and thus the ground-state energy curve of H_2, the ground state and the first excited state of H_2^+ agree with the real potential curves reasonably well, which justifies the simplified one-dimensional model in the energy point of view. The simulation grid extends over [0, 36] a.u., [−1200, 1200] a.u., [−1200, 1200] a.u. along the R, x_1, and x_2 dimensions and is sampled by 900, 8,000, and 8,000 points, respectively. In simulations, the laser wavelength and intensity are 790 nm and 9×10^{13} W/cm^2, respectively, as those used in the experiments. The laser pulse comprises 10 cycles (one-cycle ramp-on, eight-cycle constant amplitude, and one-cycle

ramp-off). We propagated the wave function after the laser pulse until the concerned physical results were converged. In boundaries of the simulation box, the absorber $\cos^{1/6}$ is applied for suppressing the unphysical reflections. Only very few dissociative ionized fragments of $H_2(1,0)$ are absorbed by the boundaries, which does not change Fig. 2*D* visibly. The signal of $H_2(1,0)$ in momentum representation was calculated by Fourier transforming the wave packet entering the following area:

$$R > 10 \text{ and } \left(\left|x_1 \pm \frac{R}{2}\right| - 5\right) \times \left(\left|x_2 \pm \frac{R}{2}\right| - 5\right) < 0,$$

from which the JES was built. Note that the potential curves in the dimensional-reduced model are not identical to the ones from the 3D model, and thus the KER in the calculations does not quantitatively agree with the measurement. We noticed that the simulated low E_N in the JES (which is not induced by rescattering but by direct absorbing extra photons after the single ionization of H_2) does not agree with the experimental measurement; however, the JES related to the rescattering dissociation agrees with the measurement quite well. To verify that the dissociation of H_2^+ is induced by the electron rescattering rather than by the direct laser–H_2^+ coupling, we artificially neglected the laser–e_2 coupling. By doing this, we obtained the similar JES in the high nuclear energy range for the wave packets that e_2 is final attached to one of the nuclei (see *SI Text* for details).

ACKNOWLEDGMENTS. We acknowledge Kenichi Ishikawa for stimulated and fruitful discussions, and Konstantin Dorfman for careful reading of the manuscript. Simulations were performed on the π supercomputer at Shanghai Jiao Tong University. This work is supported by National Natural Science Foundation of China Grants 11425416, 61690224, 11621404, 11322438, 11574205, 11327902, 11421064, 11704125, and 11761141004; Shanghai Sailing Program Grants 16YF1402900 and 17YF1404000; the 111 Project of China Grant B12024; and Innovation Program of Shanghai Municipal Education Commission Grant 2017-01-07-00-02-E00034.

1. Agostini P, Fabre F, Mainfray G, Petite G, Rahman NK (1979) Free-free transitions following six-photon ionization of xenon atoms. *Phys Rev Lett* 42:1127–1130.
2. Giusti-Suzor A, He X, Atabek O, Mies FH (1990) Above-threshold dissociation of H_2^+ in intense laser fields. *Phys Rev Lett* 64:515–518.
3. Bucksbaum PH, Zavriyev A, Muller HG, Schumacher DW (1990) Softening of the H_2^+ molecular bond in intense laser fields. *Phys Rev Lett* 64:1883–1886.
4. Orr PA, et al. (2007) Above threshold dissociation of vibrationally cold HD^+ molecules. *Phys Rev Lett* 98:163001.
5. McKenna J, et al. (2008) Enhancing high-order above-threshold dissociation of H_2^+ beams with few-cycle laser pulses. *Phys Rev Lett* 100:133001.
6. Niikura H, et al. (2003) Probing molecular dynamics with attosecond resolution using correlated wave packet pairs. *Nature* 421:826–829.
7. Kling MF, et al. (2006) Control of electron localization in molecular dissociation. *Science* 312:246–248.
8. Wu J, et al. (2013) Electron-nuclear energy sharing in above-threshold multiphoton dissociative ionization of H_2. *Phys Rev Lett* 111:023002.
9. Zhang W, et al. (2016) Photon energy deposition in strong-field single ionization of multielectron molecules. *Phys Rev Lett* 117:103002.
10. Sun X, et al. (2016) Vibrationally resolved electron-nuclear energy sharing in above-threshold multiphoton dissociation of CO. *Phys Rev A* 94:013425.
11. Madsen CB, Anis F, Madsen LB, Esry BD (2012) Multiphoton above threshold effects in strong-field fragmentation. *Phys Rev Lett* 109:163003.
12. Silva REF, Catoire F, Rivière P, Bachau H, Martín F (2013) Correlated electron and nuclear dynamics in strong field photoionization of H_2^+. *Phys Rev Lett* 110:113001.
13. Liu K, Lan P, Huang Ch, Zhang Q, Lu P (2014) Revealing correlated electronic and nuclear dynamics in molecules with energy-resolved population imaging. *Phys Rev A* 89:053423.
14. Yue L, Madsen LB (2016) Inter- and intracycle interference effects in strong-field dissociative ionization. *Phys Rev A* 93:031401.
15. Palacios A, González-Castrillo A, Martín F (2014) Molecular interferometer to decode attosecond electron-nuclear dynamics. *Proc Natl Acad Sci USA* 111:3973–3978.
16. Ranitovic P, et al. (2014) Attosecond vacuum UV coherent control of molecular dynamics. *Proc Natl Acad Sci USA* 111:912–917.
17. Dörner R, et al. (2000) Cold target recoil ion momentum spectroscopy: A 'momentum microscope' to view atomic collision dynamics. *Phys Rep* 330:95–192.
18. Ullrich J, et al. (2003) Recoil-ion and electron momentum spectroscopy: Reaction-microscopes. *Rep Prog Phys* 66:1463–1545.
19. Giusti-Suzor A, Mies FH, DiMauro LF, Charron E, Yang B (1995) Dynamics of H_2^+ in intense laser fields. *J Phys B* 28:309–339.
20. Posthumus JH (2004) The dynamics of small molecules in intense laser fields. *Rep Prog Phys* 67:623–665.
21. Ergler T, et al. (2005) Time-resolved imaging and manipulation of H_2 fragmentation in intense laser fields. *Phys Rev Lett* 95:093001.
22. Manschwetus B, et al. (2009) Strong laser field fragmentation of H_2: Coulomb explosion without double ionization. *Phys Rev Lett* 102:113002.
23. Trump C, et al. (2000) Pulse-width and isotope effects in femtosecond-pulse strong-field dissociation of H_2^+ and D_2^+. *Phys Rev A* 62:063402.
24. Xu H, et al. (2017) Observing electron localization in a dissociating H_2^+ molecule in real time. *Nat Commun* 8:15849.
25. Lindner F, et al. (2005) Attosecond double-slit experiment. *Phys Rev Lett* 95:040401.
26. Arbó DG, Ishikawa KL, Schiessl K, Persson E, Burgdörfer J (2010) Intracycle and intercycle interferences in above-threshold ionization: The time grating. *Phys Rev A* 81:021403.
27. Walker B, et al. (1994) Precision measurement of strong field double ionization of helium. *Phys Rev Lett* 73:1227–1230.
28. Becker W, Liu X, Ho PJ, Eberly JH (2012) Theories of photoelectron correlation in laser-driven multiple atomic ionization. *Rev Mod Phys* 84:1011–1043.
29. Sun X, et al. (2014) Mechanisms of strong-field double ionization of Xe. *Phys Rev Lett* 113:103001.
30. Zuo T, Bandrauk AD (1995) Charge-resonance-enhanced ionization of diatomic molecular ions by intense lasers. *Phys Rev A* 52:R2511–R2514.
31. Seideman T, Ivanov MY, Corkum PB (1995) Role of electron localization in intense-field molecular ionization. *Phys Rev Lett* 75:2819–2822.
32. Alnaser AS, et al. (2003) Rescattering double ionization of D_2 and H_2 by intense laser pulses. *Phys Rev Lett* 91:163002.
33. Niikura H, et al. (2002) Sub-laser-cycle electron pulses for probing molecular dynamics. *Nature* 417:917–922.
34. Tong XM, Zhao ZX, Lin CD (2003) Probing molecular dynamics at attosecond resolution with femtosecond laser pulses. *Phys Rev Lett* 91:233203.
35. Alnaser AS, et al. (2004) Laser-peak-intensity calibration using recoil-ion momentum imaging. *Phys Rev A* 70:023413.
36. Li Z-C, He F (2014) Ab initio non-Born-Oppenheimer simulations of rescattering dissociation of H_2 in strong infrared laser fields. *Phys Rev A* 90:053423.
37. Saugout S, Cornaggia C, Suzor-Weiner A, Charron E (2007) Ultrafast electronuclear dynamics of H_2 double ionization. *Phys Rev Lett* 98:253003.